POD ANALYSIS OF COHERENT STRUCTURES AND AEROACOUSTIC SOURCES IN A TURBULENT FLOW OVER A NACA0012 AIRFOIL

Jean Helder Marques Ribeiro, jean.marques@fem.unicamp.br[1]
William Roberto Wolf, wolf@fem.unicamp.br[1]

[1]University of Campinas, Campinas, SP, 13083-970, Brazil

Abstract: *Turbulence is a flow regime characterized by chaotic flow with three-dimensional vorticity and broad range of frequencies and spatial scales. Large Eddy Simulations (LES) are capable to solve the most energy containing large scales of the flow while filtering the dissipative small ones. Extracting physical and useful information from LES data requires the use of statistical analysis. A high-fidelity numerical simulation database of low Mach number flow past a NACA0012 airfoil is investigated in the present work. Although turbulence is three-dimensional, fully turbulent flows may have coherent structures with two-dimensional characteristics. In the present studies, two-dimensional aeroacoustic sources in the near wake region generate tonal noise. These sources are identified on acoustic field, but are not easily visualized in the hydrodynamic field. A three-dimensional vectorial Proper Orthogonal Decompostion (POD) is constructed for the present compressible flow simulations to identify coherent structures near the trailing edge. Norms are defined based on volume integrals of turbulent kinetic energy or pressure. The different structures captured by both norms are presented and discussed via a two-dimensional analysis. The most energy containing POD modes are capable of capturing large two-dimensional coherent structures appearing due to the blunt trailing edges. Farfield analysis is performed using the Ffowcs-Williams and Hawkings Analogy.*
Keywords: *POD, LES, Aeroacoustics, Turbulence, Coherent Structures*

1. INTRODUCTION

Aerodynamic lifting devices are known for its intense noise scattering and surface pressure fluctuations in a broad range of scales (Wang and Moin, 2000). This problem is encountered in a wide range of engineering applications where low-noise emitted from turbulence-solid body interaction is desired, rotor blades, turbines, pumps, aerodynamic profiles, fans, *etc*. The physics of noise scattering is mainly associated with unsteady pressure fluctuations associated to unsteady aerodynamic loads generated as air flows past and solid body, *e. g.*, an airfoil (Wolf, Azevedo and Lele, 2012). Brooks, Pope and Marcolini (1989) experiments were used to identify the main sources of airfoil noise, being them related to the flow field, namely turbulent and laminar boundary layer, separation-stall noise and tip vortex noise, or related the solid body geometry, as it is for trailing edge bluntness. In addition, Lockard and Lilley (2004) identified the trailing edge noise as the main aeroacoustic source in airfoil noise problem. In order to correctly analyze and identify aeroacoustic sources as well as understand the physics involved in coherent structures, well resolved turbulence data is needed, so variables fluctuations from unsteady aerodynamics are correctly computed.

Analyzing coherent structures in well-resolved turbulence, however, is not a simple task, despite it is indeed and old dream for physicists and engineers. The earliest works on flow visualization were performed by Brown and Roshko (1974), where shadowgraphs revealed convection at almost constant speed of an organized vortex-like quasi-2D coherent structure. In 1981, Cantwell reviewed research on turbulent flows, discussing possible ways to investigate organized structures dynamics. The definition of coherent structures as fluid mass with instantaneously correlated vorticity over space was given by the works of Hussain (1980, 1983 and 1986), which also characterized vorticity as characteristic measure of coherent structures. Hussain proposed as well a decomposition of fluid flow into mean flow, coherent and incoherent turbulence, for a better understanding of the origins and dynamics of the problem. The first proposal for investigating coherent structures without the dependence of a conditional criteria was proposed by John Lumley (1967 and 1970) as the Proper Orthogonal Decomposition (POD). Briefly, POD uses second-order statistics to extract large energy-containing structures from turbulence. Mathematical basis will be discussed further in Section 4.

Despite of its early introducing in fluid mechanics, POD has only gained attention recently, specially for its use in reduced-order modelling (ROM). For example, Rowley (2002) performed POD on flow past a two-dimensional cavity in order to use Galerkin Projection for model and reduce Navier-Stokes equations to a low-dimensional system of odinary differential equations (ODE's). Also, Nagarajan *et al.* (2009), studied the compressible cavity problem using POD coupled with ROM for flow control. Podvin (2009), Podvin *et al.* (2010) and Podvin and Sergent (2012) made use of POD for investigating the dynamics of turbulence in near-wall region for a open cavity problem with well-resolved turbulence data, also using corrections for time-coefficients, when information domain is different from the total fluid domain. In acoustics, the work of Freund and Colonius (2009) is a strong reference for understanding how POD can be used to investigate the dynamics of large coherent structures in homogeneous jet flow and the usage of POD modes for acoustic propagation and extracting noise sources.

Wolf *et al.* (2012 and 2013) presented acoustic results with a tonal noise on a NACA0012 airfoil at 5° at low Mach Number configuration, which agrees with experimental results from Brooks *et al.* (1989). The tonal noise is said to be related to the presence of large energy-containing elongated two-dimensional coherent structures, aligned in spanwise

direction. Even though, the turbulent field on the vortex wake makes it difficult to state this affirmation for the case. So, POD will be used for decomposing the flow field and identifying coherent structures and aeroacoustic sources.

This paper is organized as follows. The flowfield is re-written on a spanwise-mean two-dimensional (2D) flow for filtering the three-dimensional (3D) turbulent structures, that have poor noise scattering energy. Modal decomposition using POD is applied to the 2D flowfield in order to understand the influence of the most energy containing modes in far-field noise scattering. Comparison between direct point measurement and aeroacoustic analogies developed from Curle (1955) and Ffowcs-Williams and Hawkings (1969) (FW-H) are compared on 2D results, mean-spanwise and reconstructed flowfield from POD for different modes. Furthermore, a 3D analysis of POD is conducted. Using the acoustic field as the information domain for the POD norm, elongated 2D coherent structures responsible for noise scattering are identified near the trailing edge. Correlation of Lighthill Stress Tensor in turbulent flowfield and pressure on airfoil surface along Z-direction are analyzed to understand the dynamics of coherent structures in the present case. The 3D results are analyzed among the 2D results for identifying the physical phenomena responsible for tonal noise in the studied case.

2. NUMERICAL DATABASE

The numerical data is used to study sound generation by turbulent boundary layer on the suction side and a laminar boundary layer on he pressure side as they are convected past the round trailing edge of a NACA0012 airfoil. The angle of atack is 5° . The defined Reynolds Number based on airfoil chord length c is $Re_c = 408\ 000$ and the free-stream Mach Number is $M_\infty = 0.115$. The simulation was resolved with a sixth-order compact scheme with some adjustment near boundaries and using a high-wavenumber compact filter proposed by Lele (1992). The numerical scheme for spatial discretization is a sixth-order-accurate compact scheme from Nagarajan *et al.* (2003) implemented in a staggered grid. The overset mesh uses a fourth-order-accurate Hermite interpolation between grid zones as described by Bhaskaran and Lele (2010). Fluid equation time integrals were performed with fully-implicit second-order scheme of Beam and Warming (1978) in near-wall region. Far from solid boundaries, a third-order Runge-Kutta scheme is used for time-marching. Further reference on numerical schemes used are are given in Wolf *et al.* (2012). As the numerical schemes used are high-order-accurate, a tripping had to be used to perform transition to turbulence in the suction side of the airfoil. In order to minimize perturbations influence on flow field, the transition was performed via suction-blowing. The steady suction was performed over $0.150 \leq {}^{x}/_{c} \leq 0.175$ and blowing over $0.175 \leq {}^{x}/_{c} \leq 0.200$. Suction and blowing are consant, steady and have the same magniude in order to guarantee conservation of mass. The suction and blowing magnitude is constant over $0.01 \leq {}^{z}/_{c} \leq 0.09$ with $|U_{blowing}| = |U_{suction}| = 0.03U_\infty$.

As shown in Fig. 1 with poor resolution (8-grid point skip), the grid setup is defined as an overset mesh with a backround grid (*black* lines) and a body-fited O-grid (*red* lines). The Cartesian background structured grid zone has 896 $\times$ 511 $\times$ 64 grid points in streamwise, transversal and spanwise directions, respectively. The resolution is kept uniform around the body-fited O-grid to avoid affecting the order of accuracy of the method near the interpolation region. In turn, the O-grid has 960 $\times$ 125 $\times$ 128 grid points in parallel to airfoil surface, normal to airfoil surface and spanwise directions, respectively. Figure 1 also shows that grid points distribution is not uniform over the airfoil in order to resolve turbulent structures that are formed over the suction side.

(a) (b)

Figure 1: **Mesh Details of Numerical Data. (a) full-view of computational grid with 8-grid point skip. (b) detailed view on computational grid over airfoil with 8-grid point skip.**

The spanwise width for the present LES data was set to approx. $L_{z-LES} = 0.1c$ in order to guarantee correlation decay. Experiments with the same configuration were performed by Brooks *et al.* (1989) using a spanwise width 30 times bigger and different types of tripping the boundary layer. Nevertheless, numerically, the overset grid did not have the same spanwise width for the background and the body-fited O-grid. Considering z as the spanwise direction, according to Fig. 1, grid 1 as the body-fitted O-grid and grid 2 as the background grid, $L_{z-grid1} = 0.0992c$ and $L_{z-grid2} = 0.0984c$. Summarizing, Δz size of the grid is not proportional in span direction and a Fourier Transform in z-direction over the entire domain would result in different wavenumbers for background and body-fitted O-grid mesh. The setback of this small difference will be presented in Section 4.

3. ACOUSTIC ANALOGY

The aeroacoustic equations derived from Lighthill (1952) can be expanded to account different types of sound sources in the flow field. In this context, the general Ffowcs-Williams and Hawkings (1969) (FW-H) acoustic analogy is used for

noise predictions. The integral formulation in frequency domain can be written as

$$\left[\hat{p'}\,H\left(f\right)\right] = -\int_{f=0}\left[i\omega\hat{Q}\left(\mathbf{y}\right)G\left(\mathbf{x},\mathbf{y}\right) + \hat{F}_i\left(\mathbf{y}\right)\frac{\partial G\left(\mathbf{x},\mathbf{y}\right)}{\partial y_i}\right]dS - \int_{f>0}\hat{T}_{ij}H\left(f\right)\frac{\partial^2 G\left(\mathbf{x},\mathbf{y}\right)}{\partial y_i \partial y_j}dV\ , \tag{1}$$

where $i = \sqrt{-1}$, p' is the acoustic pressure, ω is the angular frequency, $\mathbf{y} = (y_1, y_2, y_3)^t$ is the source position, $\mathbf{x} = (x_1, x_2, x_3)^t$ is the observer's position. Hat over variables $\hat{(\cdot)}$ means it's in frequency domain. The $f = 0$ term represents the FW-H surface and $H\left(f\right)$ is the Heaviside function defined as $H\left(f\right) = 1$, if $f > 0$, and $H\left(f\right) = 0$, if $f < 0$. Monopole $\hat{Q}\left(\mathbf{y}\right)$ and dipole $\hat{F}_i$ acoustic sources are given by

$$Q = \left[\rho\left(u_i + U_i\right) - \rho_0 U_i\right]^{\partial f}/_{\partial x_i}\ , \tag{2}$$

$$F_i = \left[p'\delta_{ij} - \tau_{ij} + \rho\left(u_i - U_i\right)\left(u_j + U_j\right) - \rho_0 U_i U_j\right]^{\partial f}/_{\partial x_i}\ . \tag{3}$$

Here, u_i represents a Cartesian fluid velocity vector and U_i is the FW-H surface velocity vector, ρ_0 is the free-stream density, p' is the acoustic pressure, p is pressure, δ_{ij} is the Kronecker delta (which is 0 if $i \neq j$ and 1 if $i = j$) and τ_{ij} is the viscous stress tensor. Quadrupole sources are defined as

$$T_{ij} = \rho u_i u_j + \left(p1 - c_0^2\rho^{'}\right)\delta_{ij} - \tau_{ij}\ , \tag{4}$$

where c_0^2 is the free-stream sound speed. If one considers mean flow velocity in cartesian x-direction, the three-dimensional Green's function accounting to convective effects is given by

$$G\left(\mathbf{x},\mathbf{y}\right) = -\frac{exp\left\{-ik\left[\sqrt{\left(x_1 - y_1\right)^2 + \left(1 - M^2\right)\left[\left(x_2 - y_2\right)^2 + \left(x_3 - y_3\right)^2\right]} - M\left(x_1 - y_1\right)\right]/\left(1 - M^2\right)\right\}}{4\pi\sqrt{\left(x_1 - y_1\right)^2 + \left(1 - M^2\right)\left[\left(x_2 - y_2\right)^2 + \left(x_3 - y_3\right)^2\right]}}\ . \tag{5}$$

In this equation, k is the wavenumber, M is the free-stream Mach Number defined as $M \equiv U_1/c_0$. The Eq. 5 can be used for two-dimensional cases, considering $x_3 = y_3$. In the present work, the FW-H surface is computed over the solid airfoil surface and because of this assumption, Eq. 1 integrals are computed over a solid body only. In this way, $u_i = U_i$ for both dipole and monopole sources, reducing Eqs. 6 and 7 to

$$Q = -\rho_0 U_i{}^{\partial f}/_{\partial x_i}\ , \tag{6}$$

$$F_i = \left[p^{'}\delta_{ij} - \tau_{ij} + \rho_0 U_i U_j\right]^{\partial f}/_{\partial y_i}\ . \tag{7}$$

So, monopole sources and the second term of the dipole sources are now stationary, having no influence in frequency domain analysis. For Low-Mach number flows and, due to the fact that FW-H surface is considered a solid body over the airfoil, the quadrupole sources will be neglected and Eq. 1 can be re-writen as it has already been defined by Curle (1955), as the Curle's Analogy

$$\hat{p'}\left(\mathbf{x}\right) = -\int_{Surf}\hat{p'}\left(\mathbf{y}\right)n_i\frac{\partial G\left(\mathbf{x},\mathbf{y}\right)}{\partial y_i}dS\ . \tag{8}$$

The surface integral appearing on Eq. 8 is computed along the scattering body surfaces and dipole sources are define only as $\hat{F}_i = \hat{p'}n_i$, with n_i being the normal vector pointing outside the airfoil surface. The Hanning filter proposed by Lockard (2000) is used to guarantee conservation of the dipole sources energy before transforming data to frequency domain.

4. PROPER ORTHOGONAL DECOMPOSITION

Turbulent flows are composed of a wide range of scales and frequencies and identifying coherent structures and its dynamic behavior is not always an easy task in space-time domain. Therefore, many techniques for domain decomposition, modal decomposition and statistical method have been used in order to expand the knowledge on turbulence. Figure 2 shows a plot of the turbulent flow over a NACA0012 airfoil on space-time domain that will be used in the present work. One can clearly see the presence of coherent structures formed past the round trailing edge due to the interaction between the laminar boundary layer on the pressure side and the full-turbulent boundary layer on the suction side. However, it is not easy to understand its behavior, and some pos-processing is necessary in order to filter and decompose different scales to understand its dynamic behavior separately. Since the 1990s, modal decomposition has gained importance for analyzing unsteady aerodynamics, as done first by Hall (1994) and later by Dowell *et al.* (1998).

One of many modal decomposition techniques is the Proper Orthogonal Decomposition (POD) that was first proposed by Lumley (1967) as a modal decomposition technique for unsteady flowfields, specially for turbulent coherent structures analysis. We'll make a brief discussion on main features of POD, for further details and mathematical formulation the

(a) (b)

Figure 2: **Turbulent boundary layer flow field on z-vorticity iso-surfaces and pressure contours at time t = 95.45 s. (a) over the entire airfoil. (b) detailed view on convected eddies past the round trailing edge.**

works of Rowley (2002), Cordier and Bergmann (2003), Freund and Colonius (2009), Andrianne *et al.* (2009) and Podvin *et al.* (2010) are strongly recommended.

In POD, the vector of flow quantities $\mathbf{q}(\mathbf{x},t)$, function of space and time, is decomposed as a sum of the mean flow quantities $\bar{\mathbf{q}}(\mathbf{x},t)$ and the expansion of vector-valued spatial eigenfunctions $\boldsymbol{\phi}_i(\mathbf{x})$ and its time-coefficient mode amplitudes $\mathbf{a}_i(t)$ of flow quantities fluctuations $\mathbf{q}'(\mathbf{x},t)$ for a defined number of M modes

$$\mathbf{q}^*(\mathbf{x},t) = \bar{\mathbf{q}}(\mathbf{x},t) + \sum_{i=1}^{M} \mathbf{a}_i(t)\boldsymbol{\phi}_i(\mathbf{x}) \; . \tag{9}$$

There are many ways of computing $\boldsymbol{\phi}_i(\mathbf{x})$ and $\mathbf{a}_i(t)$. All of them pass through the Correlation Matrix computation. There are three widely known POD techniques: the Classical, also known as Direct Method, the Snapshot Method and the Spectral POD. Spectral POD is used when there's a homogeneous direction in the flow field, due to the fact that for homogeneous directions the POD modes are the Fourier modes. In the present work, z is a homogeneous direction, so the flow quantities vector $\mathbf{q}(\mathbf{x},t)$ could be written as

$$\mathbf{q}(x,y,z,t) = \sum_{k} \mathbf{q}_k(x,y,t) e^{2i\pi(kz/L_z)} \; , \tag{10}$$

where L_z is the periodic dimension of the flow. Nevertheless, in the present work we are focused on studying POD on the entire flow field domain. In this way, it is possible to analyze POD modes in the acoustic field. In this case, the numerical data provides a staggered grid with unequal L_z dimensions on near body and background grids, which would result in different wavenumber lengths in the homogeneous direction. So, in this case, the Spectral POD Method can not be used for the entire flow field. The Direct and the Snapshot Methods are capable of solving this problem. However, the Direct Method computes the spatial correlation matrix and averages over time. This is a good technique for experimental data, that usually have highly resolved time data and poor spatial resolution, according to Cordier and Bergmann (2003).

So, in the present work, we used the Snapshot Method. So we generalize $\mathbf{q} = (\rho, u_x, u_y, u_z, p)^t$, where $(u_x, u_y, u_z)^t$ is the velocity vector and each snapshot is a timestep at time t_i with correspondent value of $\mathbf{q}$. The Correlation Matrix C_{ij} is defined as the product of snapshots

$$C_{ij} = (\mathbf{q}'(\mathbf{x},t_i), \mathbf{q}'(\mathbf{x},t_j))_\Omega \; . \tag{11}$$

Also, we define a scaling vector $\boldsymbol{\beta} = (\beta_1, ..., \beta_5)$. The choice of the scaling factor $\boldsymbol{\beta}$ determines which norm is being used in POD analysis. A kinetic energy norm uses $\boldsymbol{\beta} = (0,1,1,1,0)$, a pressure norm uses $\boldsymbol{\beta} = (0,0,0,0,1)$ and so on. Now, consider $\mathbf{q}'(\mathbf{x},t_i) = \mathbf{q}'_i$. The scaling factor is applied in the inner product of the snapshot as follows

$$C_{ij} = \left(\mathbf{q}'_i, \mathbf{q}'_j\right)_\Omega = \int_\Omega \left[\beta_1 \rho'_i \rho'_j + \beta_2 u'_{xi} u'_{xj} + \beta_3 u'_{yi} u'_{yj} + \beta_4 u'_{zi} u'_{zj} + \beta_5 p'_i p'_j \right] dV \; , \tag{12}$$

where Ω is also known as information domain. The information domain is an important part of POD norm, as the norm is commonly defined by the $\boldsymbol{\beta}$ vector and the region Ω where it is computed. The use of information domain Ω for the norm different from the entire flow field or from one single grid, in the present case, is the main reason for not using the Spectral POD Method. This must be stated, despite os the presence of a homogeneous direction, as shown in Eq. 10. Moving on, the Proper Orthogonal Decomposition process requires the solution of the eigenvalue problem

$$\mathbf{C} = \mathbf{S}^{-1}\boldsymbol{\lambda}\mathbf{S} \, , \tag{13}$$

where $\mathbf{S}$ is the matrix of eigenvectors of $\mathbf{C}$ and $\boldsymbol{\lambda}$ are the eigenvalues of $\mathbf{C}$. As $\mathbf{C}$ is a diagonally dominant matrix, with real non-negative numbers in its diagonal, it can be solved using Singular Value Decomposition (SVD). For more details on mathematical background on SVD an its relation with POD, the work of Atwell and King (2004) is recommended. Normalization of $\mathbf{S}$ must be done in order to form an orthonormal basis of eigenvectors in the form $\mathbf{s}_i/\sqrt{\lambda_i M}$, considering $\mathbf{s}_i$ as the ith-column of the matrix $\mathbf{S}$. In this way. the spatial eigenfunctions can be defined as

$$\boldsymbol{\phi}_i\left(\mathbf{x}\right) = \frac{1}{\sqrt{\lambda_i M}} \sum_{m=1}^{M} \mathbf{q}'_i\left(\mathbf{x}\right) \mathbf{s}_i^m \; . \tag{14}$$

As the flowfield is decomposed, the spatial eigenfunctions are only space dependent. However, the mode shape amplitudes are functions of time and describe the unsteady flowfield among the spatial eigenfunctions. The mode amplitudes can be computed as

$$\mathbf{a}_i\left(t\right) = \int_{\Omega} \mathbf{q}_i'\left(\mathbf{x},t\right)\boldsymbol{\phi}_i\left(\mathbf{x}\right)\ dV\ . \tag{15}$$

Eventually, as already stated, the information domain Ω can be different from the entire flow field domain, so a more general form of computing the time coefficients of the model shape amplitudes can be used. The general formula takes into account only the eigenvectors and eigenvalues generated in solving the eigenvalue problem in Eq. 13. In this way, the mode shape amplitudes $\mathbf{a}_i\left(t\right)$ will be related to the information domain as well as the spatial eigenfunctions $\boldsymbol{\phi}_i\left(\mathbf{x}\right)$. So, in a simplified form, the mode amplitudes $\mathbf{a}_i\left(t\right)$ are computed in the following form applied to the Snapshot Method

$$\mathbf{a}_i\left(t\right) = \mathbf{s}_i\sqrt{\lambda_i M}\ . \tag{16}$$

In this way, it is possible to reconstruct the flow field with a limited number of spatial eigenfunctions and mode shape amplitudes using Eq. 9. If one reads a number M of snapshots, it is possible to generate the same number of eigenvalues and eigenfunctions. However, POD has received attention in the research area (among other things) due to its capacity of containing most of the energy of the flow field fluctuations with a few number of modes and so, compressing information of large numerical and experimental data. Even so, if one uses Eq. 9 with the same number of snapshots and modes, the reconstructed flowfield must contain 100% of the original flowfield energy. In this case,

$$\mathbf{q}^*(\mathbf{x},t) = \mathbf{q}(\mathbf{x},t)\ . \tag{17}$$

If not, using a fewer number of modes M, $\mathbf{q}^*(\mathbf{x},t)$ is considered an approximation and contain information related to the spatial eigenfunctions and mode shape amplitudes that were used to build the new vector of flow quantities $\mathbf{q}^*$. In the present work, both the results of Eq. 9 and 14 will be used to understand and detect coherent structures generated by the turbulent flow field. Also, Eq. 17 will be used as a comparison of the energy contained in the reconstructed flow field.

5. RESULTS AND DISCUSSION

5.1 Two-dimensional POD and FW-H

In order to filter three-dimensional fluctuations in the flow field, a spanwise direction mean was performed, resulting on a two-dimensional set of flow data. Fig. 3 shows the mean 2D results plot for x-momentum and the RMS value. This shows that fluctuations on spanwise direction are small, still they must not be neglected.

(a) (b)

Figure 3: **Two-dimensional spanwise statistical filtering treatment results shown as (a) spanwise-mean x-momentum. (b) spanwise-RMS x-momentum.**

Even so, POD 2D can provide insights on the correct norms for the case. In the present work, both pressure and kinetic energy based norms are used. Figure 4 shows that pressure-based norm has higher magnitude of pressure fluctuations in farfield. Even modes with less energy for pressure norm have a wave-like form in acoustic propagation, which is better when reconstructing flowfield for acoustic scattering. As presented, modes 11 for both norms have disturbances in wake vortex, which is a regular behavior for less energetic modes.

As already discussed, POD can contain most of the energy of the flowfield in a few number of modes. Figure 5 presents the energy contained in the first 200 modes and the sum of the energy for a given number of modes. Pressure-based norm converges faster, which shows that for a smaller number of POD modes, the reconstructed flow-field would have more energy than using the kinetic energy norm.

The case being analyzed has a tonal noise which is characterized by the most energetic mode, as show in Fig. 6. Using the first 2 modes, both norms are able to reconstruct the tonal noise in near and far-field.

Figure 6(a) also presents a comparison between the direct point measurement of pressure fluctuations in sound pressure level (SPL) scale in nearfield and the use of the Ffowcs-Williams and Hawkings analogy for acoustic predictions at the same point. Important to notice that the use of spectral averages, instead of the complete set of time data for Discrete Fourirer Transform could give better results and approximate FW-H and direct results. as this was not done in the present work, small differences can be related to non-softened spectra results by spectral averages. Figure 7 describes how POD is used to filter high frequency perturbations, while retaining information at characteristic wavenumbers with regards to the most energetic coherent structures of the flow field.

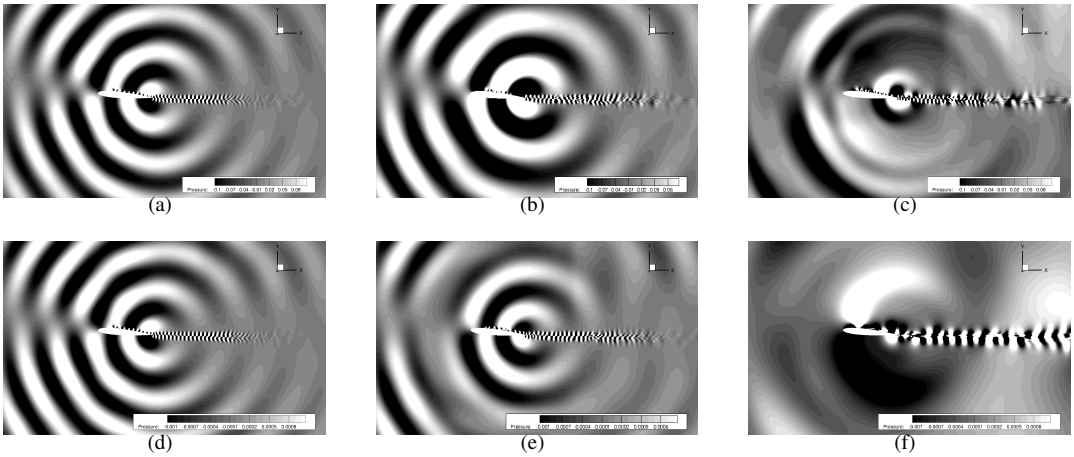

Figure 4: **Pressure contours for spatial eigenfunctions using pressure-based norm (a) mode 1, (b) mode 6 and (c) mode 11. For kinetic energy based norm (d) mode 1, (e) mode 6 and (f) mode 11.**

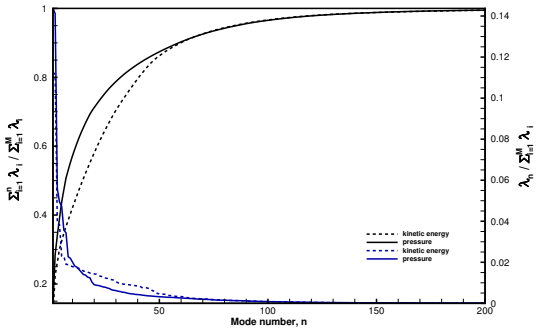

Figure 5: $\boldsymbol{\lambda}_i$ **for the first 200 modes for pressure and kinetic-energy based norms, shown as the total of energy up to a given number of modes (black lines) and as the individual percentage of total flow field energy (blue lines).**

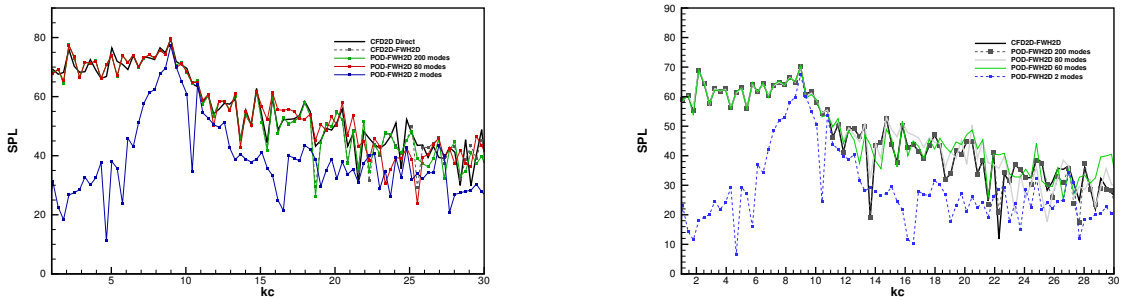

(a) (b)

Figure 6: **Pressure-based norm results for acoustic scattering spectra with direct point measure and acoustic analogy presented in Eq. 8 for (a) nearfield and (b) farfield regions.**

Despite of preserving the physics of the original flowfield, the reconstructed flowfield not always match the propagation in all directions. For bigger wavelengths, the reconstruction with a few number of modes has more influence in the magnitude of p'. For 2 modes, only the tonal noise is well represented as shown in Fig. 8(b). In smaller wavelengths, the reconstructed flowfield with a few number of modes affects the physics of the acoustic scattering and the shapes of p' plots are distorted in Figs. 8(c) and (d).

5.2 Three-dimensional POD and FW-H

In 3D POD, he Eq. 12 was used with Ω as the region upward and downward the airfoil without hydrodynamic turbulence and $\boldsymbol{\beta}$ as a pressure-based norm, which makes convergence of POD modes faster. The first POD mode presented in Fig. 9 shows two-dimensional elongated coherent structures formed near the trailing edge. Those coherent structures are considered the main source of noise in the present case.

Aeroacoustic sources in turbulent field can be identified via Lighthill Tensor as defined previously in Eq. 4. The presence of correlated structures near the trailing edge is shown in 3D POD modes in Fig. 10. As shown, POD modes 1

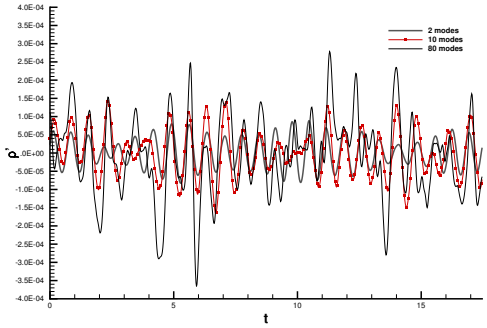

Figure 7: **Density fluctuations $0.1c$ far from trailing edge showing how the most energy containing POD modes are able to filter high frequencies.**

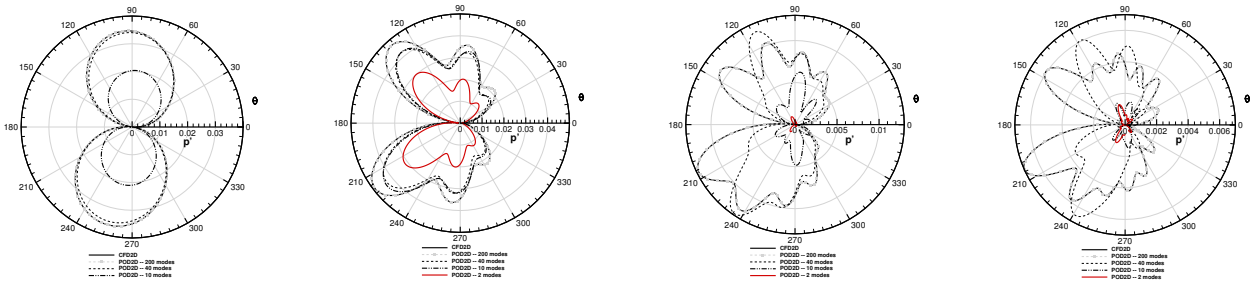

(a) (b) (c) (d)

Figure 8: **$\mathbf{p'}$ directivity plots for observer's location at $\mathbf{r = 7.9c}$ from trailing edge, for 2D CFD and 2D POD reconstruction with different sum of modes and wavenumbers: (a) $\mathbf{kc = 2.52}$; (b) $\mathbf{kc = 8.62}$; (c) $\mathbf{kc = 14.38}$; (d) $\mathbf{kc = 18.33}$.**

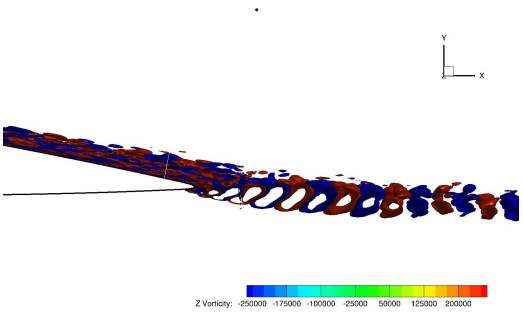

Figure 9: **Isosurfaces of z-vorticity at trailing edge showing two-dimensional coherent structures on most energy containing POD mode (17% of total energy).**

and 2, the most energy containing ones capture the presence of large structures in near wake vortex region, which stands for the paramount importance of quadrupole sources in acoustic scattering for the present case.

Dipole aeroacoustic sources are also important for the present case. They were the only ones computed in Section 5.1 Dipole sources are related to pressure fluctuations in airfoil surface. Fig. 11 shows how pressure is correlated in airfoil surface at some points in suction side. These structures in the most energy containing POD mode are related to the acoustic scattering of dipole sources. Pressure side is highly correlated but that happens because flow is laminar on this side.

6. CONCLUSIONS

The present investigation is focused in decomposing the turbulent flow field, in order to investigate the aeroacoustic sources and coherent structures formed by the interaction of laminar and turbulent boundary layers near the blunt trailing edge.The modal decomposition is performed using the Proper Orthogonal Decomposition (POD) and the acoustic predictions are performed using the Ffowcs-Williams and Hawkings acoustic analogy accounting only for surface pressure fluctuations, also known as Curle's acoustic analogy.

The two-dimensional implementation of POD is analyzed and lead to important conclusions. For example, the pressure-based norm has shown to be more efficient in acoustic propagation analysis and has faster convergence. Also, POD is presented not as a high frequency filter, but as a energy filter. The most energetic coherent structures are found in the most energy containing modes, despite of having higher or lower frequencies. The tonal noise in the sound pressure level spectra is reconstructed in the use of only 2 modes. Important to notice that the shape of directivity of sound

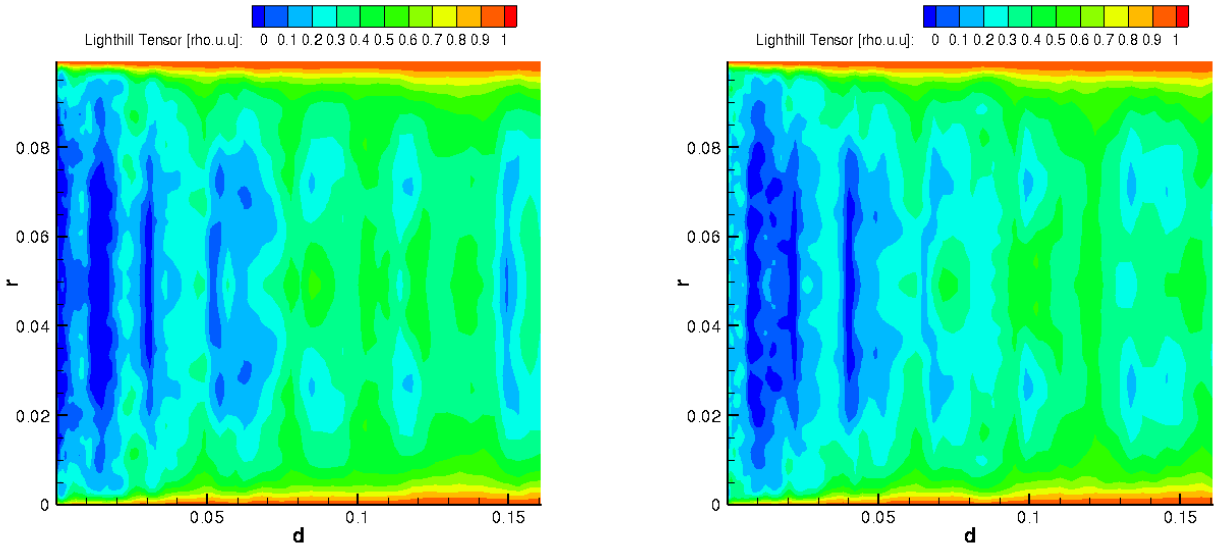

(a) (b)

Figure 10: **Lighthill Tensor T_{11} correlation at wake vortex region. The r is the point-correlation distance in Z-direction and d is the mean distance from airfoil surface. (a) POD mode 1; (b) POD mode 2.**

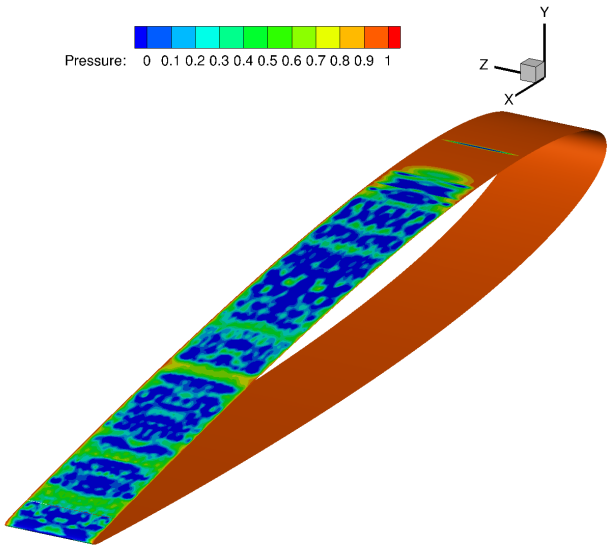

Figure 11: **Pressure Correlation at airfoil surface for POD mode 1. Z-direction represents r, the point-to-point distance in spatial correlation.**

scattering is altered depending on the number of modes used for POD reconstruction.

For three-dimensional POD, results have shown that the first POD modes have important information about acoustic sources in airfoil surface and in near wake region. Both regions are related to important aeroacoustic sources, dipole and quadrupole. The 3D POD shows large elongated coherent structures in near wake region which are not easily identified in original flowfield.

7. ACKNOWLEDGEMENTS

The authors gratefully acknowledge the partial support for this research provided by Conselho Nacional de Desenvolvimento Científico e Tecnológico, CNPq, under the Research Grant No. 470695/2013-7. The work was also supported by Fundação de Amparo à Pesquisa do Estado de São Paulo, FAPESP, under the Research Grant No. 2013/03413-4. The computational resources and technical support provided by Centro Nacional de Processamento de Alto Desempenho, CENAPAD-SP, under Project No. 551, are also gratefully acknowledged. The first author is supported by a CAPES MSc. scholarship, which is also acknowledged.

8. REFERENCES

Andrianne, T., Ligot, J. and Dimiriadis, G., 2009. "Proper orthogonal decomposition of unsteady aerodynamic flows". Research report, Department of Aerospace and Mechanical Engineering of University of Liege, Liège, Belgium.

Atwell, J.A. and King, B.B., 2004. "Reduced order controllers for spatially distributed systems via prper orthogonal decomposition". *SIAM J. Sci. Comput.*, Vol. 26, pp. 128–151.

Beam, R.M. and Warming, R.F., 1978. "An implicit factored scheme for the compressible navier-stokes equations". *AIAA journal*, Vol. 16, No. 4, pp. 393–402.

Bhaskaran, R. and Lele, S.K., 2010. "Large eddy simulation of free-stream turbulence effects on heat transfer to a high-pressure turbine cascade". *Journal of Turbulence*, , No. 11, p. N6.

Brooks, T.F., Pope, D.S. and Marcolini, M.A., 1989. "Airfoil self-noise and prediction". Technical report, 1218 NASA Reference Publication.

Brown, G.L. and Roshko, A., 1974. "On density effects and large structure in turbulent mixing layers". *Journal of Fluid Mechanics*, Vol. 64, No. 04, pp. 775–816.

Cantwell, B., 1981. "Organized motion in turbulent flow". *Ann. Rev. Fluid Mech*, Vol. 13, pp. 457–515.

Cordier, L. and Bergmann, M., 2003. "Proper orthogonal decomposition: An overview". Technical report, Laboratoire d'Energétique et de Mécanique Théorique et Appliquée, Vandoeuvre-lès-Nancy, France.

Curle, N., 1955. "The influence of solid boundaries upon aerodynamic sound". *Proceedings of the Royal Society of London Series A*, Vol. 231, pp. 505–514.

Dowell, E.H., Hall, K.C. and Romanowski, M.C., 1998. "Eigenmode analysis in unsteady aerodynamics: Reduced order models". *Applied Mechanics Reviews*, Vol. 50, No. 6, pp. 371–385.

Ffowcs-Williams, J.E. and Hawkings, D.L., 1969. "Sound generated by turbulence and surfaces in arbitrary motion". *Philosophical Transactions of the Royal Society of London Series A*, Vol. 264, pp. 321–342.

Freund, J.B. and Colonius, T., 2009. "Turbulence and sound-field pod analysis of a turbulent jet". *International Journal of Aeroacoustics*, Vol. 8, No. 4, pp. 337–354.

Hall, K.C., 1994. "Eigenanalysis of unsteady flows about airfoils, cascades, and wings". *AIAA Journal*, Vol. 32, No. 12, pp. 2426–2432.

Hussain, A.K.M.F., 1980. "Coherent structures and studies of perturbed and unperturbed jets". *Lecure Notes in Physics*, Vol. 136.

Hussain, A.K.M.F., 1983. "Coherent structures – reality and myth". *Phys. of Fluids*, Vol. 26, pp. 2816–2850.

Hussain, A.K.M.F., 1986. "Coherent structures and turbulence". *J. Fluid Mech.*, Vol. 173, pp. 303–356.

Lele, S.K., 1992. "Compact finite difference schemes with spectral-like resolution". *Journal of computational physics*, Vol. 103, No. 1, pp. 16–42.

Lighthill, M.J., 1952. "On sound generated aerodynamically, part 1: General theory". *Proceedings of the Royal Society of London Series A*, Vol. 211, pp. 564–587.

Lockard, D.P., 2000. "An efficient, two-dimensional implementation of the ffowcs-williams and hawkings equation". *Journal of Sound and Vibration*, Vol. 229, pp. 897–911.

Lockard, D.P. and Lilley, G.M., 2004. "The airframe noise reduction challenge". Tech. report 213013, NASA Report.

Lumley, J.L., 1967. "The structure of inhomogeneous turbulent flows". *Atmospheric turbulence and radio wave propagation*, pp. 166–178.

Lumley, J.L., 1970. *Stochastic Tools in Turbulence*. Academic Press, New York.

Nagarajan, K.K., Cordier, L., Airiau, C. and Kourta, A., 2009. "Pod based reduced order modelling of a compressible forced cavity flow". In *Proceedings of the 19th French Congress on Mechanics*.

Nagarajan, S., Lele, S.K. and Ferziger, J.H., 2003. "A robust high-order compact method for large eddy simulation". *Journal of Computational Physics*, Vol. 191, No. 2, pp. 392–419.

Podvin, B., 2009. "A proper-orthogonal-decomposition–based model for the wall layer of a turbulent channel flow". *Physics of Fluids*, Vol. 21, No. 1, p. 015111.

Podvin, B., Fraigneau, Y., Jouanguy, J. and Laval, J.P., 2010. "On self-similarity in the inner wall layer of a turbulent channel flow". *Journal of Fluids Engineering*, Vol. 132, No. 4, p. 041202.

Podvin, B. and Sergent, A., 2012. "Proper orthogonal decomposition investigation of turbulent rayleigh-bénard convection in a rectangular cavity". *Physics of Fluids*, Vol. 24, No. 10, p. 105106.

Rowley, C.W., 2002. *Modeling, Simulation and Control of Cavity Flow Oscillations*. Ph.D. thesis, California Institute of Technology.

Wang, M. and Moin, P., 2000. "Computation of trailing-edge flow and noise using large-eddy simulation". *AIAA Journal*, Vol. 38, No. 12, pp. 2201–2209.

Wolf, W.R., Azevedo, J.L.F. and Lele, S.K., 2012. "Convective effects and the role of quadrupole sources for aerofoil aeroacoustics". *Journal of Fluid Mechanics*, Vol. 708, pp. 502–538.

Wolf, W.R., Azevedo, J.L.F. and Lele, S.K., 2013. "Effects of mean flow convection, quadrupole sources and vortex shedding on airfoil overall sound pressure level". *Journal of Sound and Vibration*, Vol. 332, pp. 6905–6912.

9. RESPONSIBILITY NOTICE

The authors are the only responsible for the printed material included in this paper.